

Under construction: improving arteriovenous fistula maturation

Laboyrie, S.L.

Citation

Laboyrie, S. L. (2025, October 17). *Under construction: improving arteriovenous fistula maturation*. Retrieved from https://hdl.handle.net/1887/4270719

Version: Publisher's Version

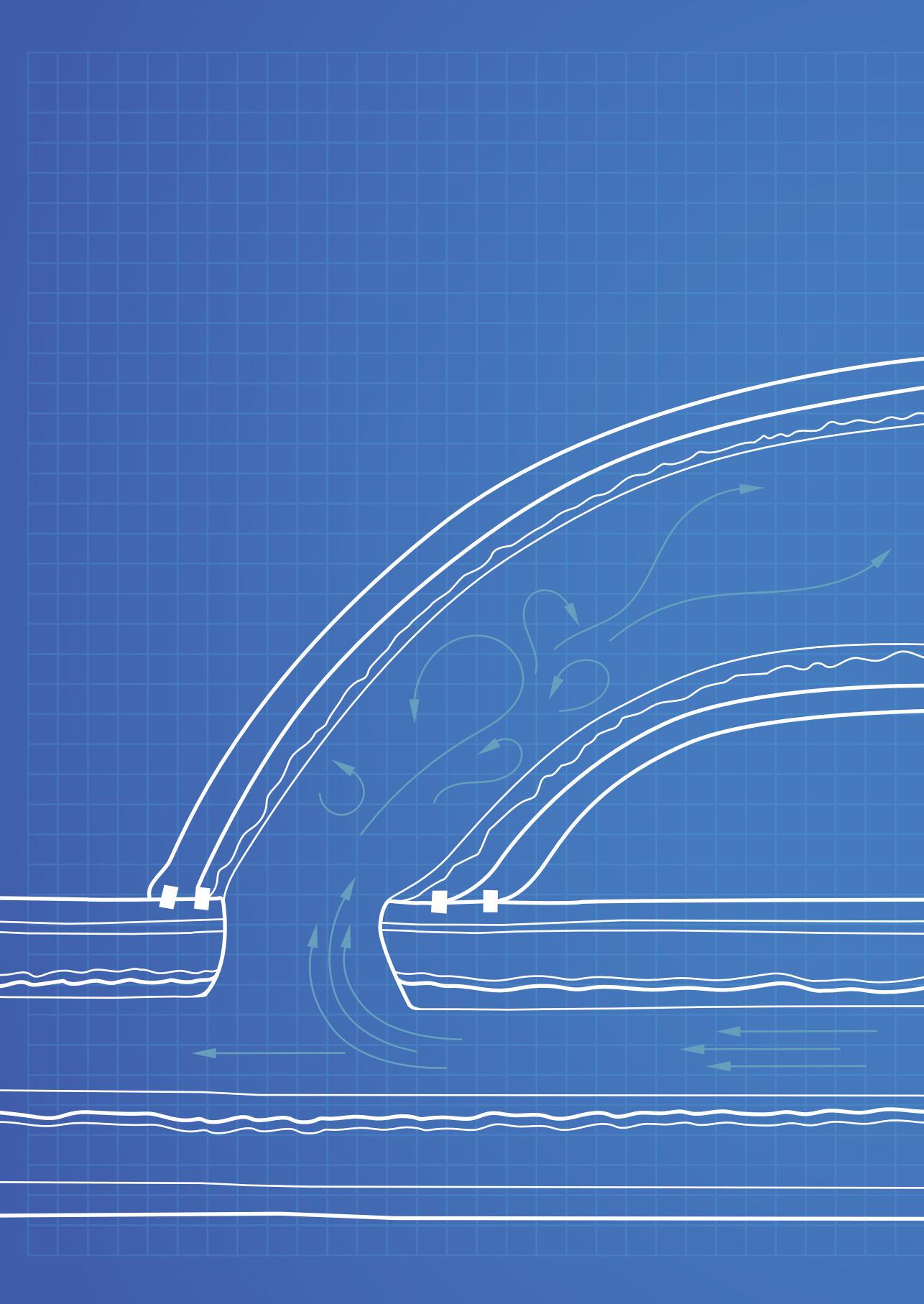
Licence agreement concerning inclusion of doctoral

License: thesis in the Institutional Repository of the University

of Leiden

Downloaded from: https://hdl.handle.net/1887/4270719

Note: To cite this publication please use the final published version (if applicable).





The impact of chronic kidney disease on arteriovenous fistula remodelling: studies in a murine model of autosomal dominant polycystic kidney disease

Suzanne L Laboyrie, Dorien JM Peters, Roel Bijkerk, Eduard P de Winter, Jacques MGJ Duijs, Juliette A de Klerk, Margreet R de Vries* and Joris I Rotmans*
*Shared last author

Accepted for publication in American Journal of Physiology - Renal Physiology

Abstract

The arteriovenous fistula (AVF) is the gold standard for hemodialysis vascular access, although inadequate vascular remodelling and intimal hyperplasia pose a major limitation. It is essential to study this in a clinically relevant model. We utilised an autosomal dominant polycystic kidney disease (ADPKD) model, the most common hereditary cause of chronic kidney disease (CKD), to study the effect of CKD on AVFs.

Jugular-carotid AVFs were created in adult B6Ola*Pkd1*^{nl/nl} (ADPKD) mice and B6Ola*Pkd1*^{+/+} litter mates. AVFs were harvested seven days post-surgery for bulk mRNA sequencing or three weeks post-surgery for histological analysis. We performed weekly AVF flow measurements using doppler ultrasound and assessed kidney morphology and function by histology and blood urea analysis. Blood pressure was measured using a tail cuff, before and six days after AVF-surgery. Longitudinal flow data was analysed using Mixed-effects model, histological data using the Mann-Whitney U test.

 $Pkd1^{nl/nl}$ mice developed cystic kidneys and elevated blood urea levels (8.7 ± 2.8 mmol/L versus 24.0 ± 3.8 mmol/L) and higher mean arterial blood pressure (92 versus 113). AVF flow in $Pkd1^{nl/nl}$ mice was consistently higher post-AVF creation (1.9-fold difference, p<0.001), with a 50% reduction in intimal hyperplasia and 30% increase in luminal AVF volume. RNA sequencing showed altered regulation of extracellular matrix in the venous ADPKD AVF, with reduced collagen deposition in the venous outflow tract. The arterial AVF wall had disruption of the elastic laminae. $Pkd1^{nl/nl}$ mice are a suitable model to study AVF remodeling in a CKD setting, resulting in enhanced luminal volume and higher AVF flow when compared to normotensive mice with normal kidney function.

New & noteworthy

This work explores the impact of chronic kidney disease (CKD) on arteriovenous fistula (AVF) remodeling using an autosomal dominant polycystic kidney disease (ADPKD) mouse model. Our findings reveal that ADPKD enhances AVF flow and luminal volume while reducing intimal hyperplasia, due to altered extracellular matrix deposition, offering new insights into the vascular AVF changes in a CKD setting. This study highlights the suitability of the ADPKD model for investigating AVF remodeling in a CKD context.

Keywords

Arteriovenous fistula, chronic kidney disease, autosomal dominant polycystic kidney disease, murine model, vascular remodelling.

Introduction

To optimise the efficacy of hemodialysis treatment for end-stage kidney failure (ESKD), a well-functioning vascular access site providing a robust blood flow supply to the dialyser is essential. While the arteriovenous fistula (AVF) is the preferred vascular access method, its frequent primary failure poses a significant challenge. Factors as inadequate outward remodelling (OR) and the occurrence of excessive stenosis or intimal hyperplasia (IH) can hinder AVF maturation, creating a bottleneck for initiating hemodialysis [1]. These vascular access-related complications lead to hospitalisations, increased morbidity, and impose a substantial burden on both patients and health care. Therefore, comprehending the process of AVF maturation failure and understanding how factors like kidney failure influence vascular remodelling post AVF surgery is crucial.

To investigate the impact of the uremic environment on AVF vascular remodelling, studies have predominantly utilized models of acute kidney failure, such as nephrectomy [2-4] or unilateral ureteral obstruction [5], L-NAME administration to induce vascular injury and hypertension [6], or diet-induced kidney failure. [7, 8] However, these acute kidney injury models fail to replicate the phenotype of ESKD, lacking the aspects of early onset kidney injury, the progressive injury associated with ESKD and hypertension —key clinical characteristics observed in many ESKD patients receiving an AVF. Consequently, a representative ESKD model for studying its effect on AVF maturation is currently lacking. However, as hypertension is argued to have a protective effect on AVF failure [9, 10], while uraemia accelerates wall thickening and IH in mice [3, 11], it is important to incorporate both these ESKD hallmarks in one model to study AVF maturation.

In the present study, we employed a clinically relevant CKD model to elucidate the impact of CKD on vascular AVF remodelling. Specifically, we utilised a well-characterised murine model of autosomal dominant polycystic kidney disease (ADPKD) [12, 13], the most common hereditary cause of kidney failure, and created AVFs between the carotid artery and jugular vein.

Our analysis included the evaluation of kidney function and blood pressure and investigating the effects of CKD on blood flow and vascular remodelling in the AVF. Acute kidney injury models showed that kidney failure mainly affected AVF remodelling through IH aggravation [3, 11]. We however hypothesised that our chronic CKD model, along with its impact on blood pressure and progressive vascular damage, affects AVF maturation mostly through medial vessel wall turnover.

Materials and methods

Animals and Study design

This study was performed in compliance with Dutch guidelines, the Directive 2010/63/EU of the European Parliament, and was approved by the Institutional Committee for Animal Welfare at the Leiden University Medical Centre. Adult $B6Ola-Pkd1^{nl/nl}$ and $B6Ola-Pkd1^{nl/nl}$ mice, aged 8 to 12 weeks and bred in our own facility, were used for the *in vivo* studies. We decided on minimal sample size using G*power calculation, where we viewed intimal hyperplasia as the main parameter. The study groups were littermates and were housed together. Every surgery session was performed blinded, and mice of the same cage – i.e. possibly both $B6Ola-Pkd1^{nl/nl}$ mice – received an AVF to minimize confounding. Due to ADPKD's genetic background, the animals could not be randomised, instead the two groups were matched for age and sex. Heterozygous littermates were excluded from the study.

The previously described ADPKD model [12, 13] with an intronic neomycin-selectable marker causing aberrant splicing of intron 1, has a hypomorphic Pkd1 allele. This results in reduced (10-20%) *Pkd1* transcript levels in kidneys of *B6Ola-Pkd1*^{nl/nl} mice compared with their wildtype *B6Ola-Pkd1*^{+/+} controls. Before AVF surgery, the mice were anesthetised via intraperitoneal injection of midazolam (5 mg/kg, Roche), medetomidine (0.5 mg/kg, Orion), and fentanyl (0.05 mg/kg, Janssen) and received unilateral AVFs, as previously described [14] between the dorsomedial branch of the external jugular vein and the common carotid artery (CCA). After surgery, anaesthesia was antagonized with atipamezole (2.5 mg/kg, Orion) and flumazenil (0.5 mg/kg, Fresenius Kabi). Buprenorphine (0.1 mg/kg, MSD Animal Health) was given after surgery for two days to relieve pain.

It should be noted that compared to previously used models on a C57BL/6 or B6.129S2 background [14, 15], we observed some challenges with anesthetising the animals prior to surgery, with delayed subconsciousness and rapid recovery from anaesthesia. Therefore, adequate monitoring of the level of anaesthesia presurgery through toe pinching was performed throughout surgery, and for some mice additional anaesthesia was administered during surgery.

Before AVF surgery, blood pressure was measured in six *Pkd1**/+ and six *Pkd1**/- mice, and in the same animals six days post AVF-surgery. All mice underwent Doppler ultrasound at baseline, day three post-surgery and then weekly. During AVF surgery (day zero) and tissue harvest at day 21, blood was retrieved to

measure blood urea levels. We assessed vascular remodelling both at the early stage, seven days post AVF surgery through RNA sequencing, to investigate which processes precede the eventual stable phase 21 days post-AVF surgery, which we assessed with histology. Kidneys from all mice were harvested to monitor cyst formation. The experimental protocol is shown in figure 1.

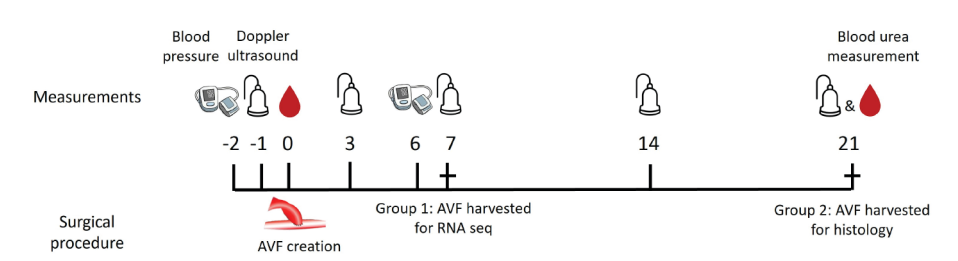


Figure 1: Experimental protocol of murine AVF studies
AVF = arteriovenous fistula, RNA seq = bulk RNA sequencing

Blood pressure measurements

Systolic and diastolic blood pressure were assessed with a non-invasive tail cuff system in conscious mice using the CODA system (Kent Scientific, Torrington, CT, USA). To minimise stress, blood pressure and ultrasound analysis were measured on separate days. Blood pressure was measured according to manufacturer's instructions two days before the AVF surgery and six days post-surgery. Animals were acclimated to the restrainer before measurements. Hereafter, 10 acclimation cycles were followed by 20 measurement cycles.

Blood urea measurements

Blood was obtained from the AVF at its creation, using Lithium Heparin capillary tubes (Abbott #52193), and at sacrifice, 21 days after surgery. Blood urea levels were determined with Reflotron Urea strips (Roche diagnostics #11200666202) on the Reflotron Plus (Roche Diagnostics, Basel, Switzerland) according to the manufacturer's protocol.

RNA isolation and RNA sequencing

Seven days post-AVF surgery, five mice per group were anesthetised as described previously and perfused with PBS through cardiac perfusion. AVFs were collected and separated into the arterial and venous segment, which were snap frozen in liquid nitrogen. RNA was isolated using the Qiagen RNeasy microkit (74004) according to manufacturer's protocol with several adjustments: adding

1% beta-mercaptoethanol to the RLT lysis buffer, performing tissue disruption and homogenisation with glass beads at 1800rpm for one minute, followed by proteinase K digestion for 10 minutes at 55 degrees Celsius. After quality control of the RNA, this resulted in n=4 for wildtype venous AVF samples and n=5 for venous AVF samples from $Pkd1^{nl/nl}$ mice. The arterial AVF samples were n= 3 for $Pkd1^{*l/n}$ and n=4 for $Pkd1^{nl/nl}$ mice. Preparation and bulk mRNA sequencing was performed at Genomescan (Leiden, The Netherlands), with 20 million PE150 reads. Total RNA was quantified and \geq 250 ng was used as input on the Illumina NovaSeq6000.

Differential Gene Expression Analysis

Differentially expressed genes (DEGs) between AVF samples, both arterial and venous, harvested seven days after surgery of *Pkd1**/+ and *Pkd1**/* mice were identified. Reads were aligned to the mouse genome (GRCm39 M33) with STAR (v2.7.7a). For the assessment of differential expression, a quasi-likelihood negative binomial generalized log-linear model was used, using R package edgeR (v3.42.4). Counts underwent normalisation through the Trimmed Mean of the M-values (TMM) method. Genes were considered differentially expressed if the observed contrast between ADPKD and controls reached statistical significance, as indicated by a false discovery rate (FDR)-adjusted P-value below 0.05. Gene set enrichment analysis was performed with R package ClusterProfiler (v.4.8.3) of Gene Ontology (ref: https://geneontology.org/). All analyses were performed using R statistics (v4.3.1). Figures were produced using the R packages ggplot2 (v3.4.4) and enrichplot (v.1.20.3), showing the data as counts per million (cpm).

Ultrasound analysis and 3D volume measurements

Ultrasound analysis was performed under isoflurane anaesthesia as described previously [15] one day before AVF surgery, and at day three and seven post AVF-creation for every animal, and day 14 and 21 for mice that were sacrificed at 21 days after surgery. The following recordings were obtained at each time point: ECG-gated Kilohertz visualisation (EKV) brightness-mode (B-mode) of the CCA afferent to the anastomosis, short-axis three-dimensional B-mode and colour Doppler, long-axis three-dimensional B-mode and colour Doppler, PW Doppler of the CCA afferent to the anastomosis. For the PW Doppler measurements, an angle of $\leq 59^\circ$ was employed. We extrapolated the diameter and thereby area of the CCA from the EKV measurements, and flow velocity from PW Doppler data. These measurements were used to define flow volume in the AVF: flow volume = (CCA diameter/2)² * π * mean flow velocity. Maximum systolic accelerations (ACCmax) were measured from PW Doppler data.

Luminal volumes of the AVFs were measured by tracing the lumen downstream of the anastomosis in the first 63 frames, each 0.04 mm apart, directly in the short-axis three-dimensional B-mode. The length of the AVF in the selected frames was also measured, using the measuring tool in VEVO lab and mid-lumen points of the traced areas. The total volume was then corrected for the total length of the AVF, allowing for the appreciation of the volume in the AVF over the first 2.5 mm downstream of the anastomosis.

Tissue harvest and processing for histology

21 days after AVF surgery, mice were anesthetized using a mixture containing midazolam (5 mg/kg, Roche), medetomidine (0.5 mg/kg, Orion), and fentanyl (0.05 mg/kg, Janssen) via intraperitoneal injection. The thorax was opened and flushed through intracardiac perfusion with PBS and thereafter formalin, whereafter the AVF and kidneys were dissected and submerged in formalin overnight, then embedded in paraffin. Since most AVF remodelling occurs in the venous outflow tract of the AVF, the first 3 perpendicular venous cross sections downstream of the anastomosis with 150-µm interval were used for morphological and immunohistochemical analysis.

Second harmonic generation

Paraffin embedded tissue was deparaffinated and rehydrated. 5 µm tissue sections were excited with a laser using an 800 nm wavelength using Multiphoton microscopy (Zeiss LSM 710). Second harmonic generation (SHG) images were obtained using a band-pass emission filter at the SHG (380-430 nm) wavelength. A wide-band pass emission filter (300–755 nm) was also used to collect the combined all two-photon excited fluorescence (TPF) signal. Collagen quantification was performed with ImageJ software by calculating SHG positive area over the total vessel area.

Staining and morphometric analysis

Kidneys were stained using Periodic acid-Schiff (PAS) staining. To verify RNA-sequencing findings at 21 days post AVF-surgery, murine AVFs were stained for Tenascin-C (Sigma Aldrich, ZRB2975) and VEGFR3 (Abcam ab317030) which is encoded by Flt4. To visualise the elastic lamina of the venous outflow tract and CCA afferent to the anastomosis, murine AVFs were stained with Weigert's elastin. Tissue within the internal elastic lamina (IEL) of the venous AVF outflow tract was defined as IH and determined using histoquant software (3DHISTECH). Slides that were used to study collagen deposition were analysed with SHG and followingly

stained for α SMA (DAKO M0851) and Vimentin (Thermo Scientific, MS-129-P1) to determine presence of collagen-producing cells.

Morphology of extracellular matrix in human renal arteries

To evaluate whether the observations in our mouse model corresponded to patient blood vessels, renal arteries were obtained post-nephrectomy. We included two patients with renal cell carcinoma with normal kidney function (control samples) and two patients with ADPKD. Specimens were obtained at the LUMC in accordance with guidelines set out by the 'Code for Proper Secondary Use of Human Tissue' of the Dutch Federation of Biomedical Scientific Societies (Federa) and conform with the principles outlined in the Declaration of Helsinki. The study was approved by the local ethical committee and the donors gave informed consent. The control samples were obtained from donors with an eGFR > 60 mL/min/1,73m². They underwent nephrectomy due to renal carcinoma and did not have metastasis or diabetes mellitus. The arterial samples were used for histological analysis to study the extracellular matrix, using a Weigert's elastin stain and Masson Trichrome staining.

Statistical analysis

Graphpad Prism 8 was used to perform statistical analysis. Normally distributed data are presented as mean ± SD. Nonparametric data are presented as the median ± interquartile range. Unpaired t test, 1-way ANOVA, Restricted Maximum Likelihood (REML), and Mann–Whitney U test (2-tailed) were used when applicable. P<0.05 is considered significant. Analyses were also separately performed for male and female mice; results can be found in the supplemental figures.

Results

Surgical outcome

36 animals received an AVF, of which 15% from the $Pkd1^{v/v}$ mice and 14% of $Pkd1^{nl/nl}$ mice were excluded from morphological analysis due to technical difficulties during surgery, such as vessel spasms or bleeding, causing early occlusion or distorted vascular remodelling of the lumen, as seen on ultrasound analysis observed at early time points such as directly or three days post-AVF surgery. 17 $Pkd1^{v/v}$ (9 female, 8 male) and 19 $Pkd1^{nl/nl}$ mice (10 female, 9 male) were included in the study.

Pkd1^{nl/nl} mice developed chronic kidney disease and hypertension

Kidneys of $Pkd1^{nl/nl}$ mice were visibly larger in size compared to control mice and presented with cysts throughout the kidneys (figure 2A, B). Furthermore, impaired kidney function was observed in $Pkd1^{nl/nl}$ mice, with elevated blood urea levels at AVF-creation (24.0 ± 3.8 mmol/L, Figure 2C), which remained stable over the three-week study period (23.1 ± 3.7 mmol/L), compared to $Pkd1^{t/t}$ mice (8.7 ± 2.8 mmol/L at AVF-creation and 8.3 ± 3.4 mmol/L at 21 days). $Pkd1^{nl/nl}$ mice also developed hypertension, with elevated mean arterial blood pressure (MAP) at both timepoints compared to $Pkd1^{t/t}$ mice. $Pkd1^{t/t}$ mice, demonstrated a 20% (113 vs 92, p= 0.00001) and 30% (100 vs 76, p=0.002, Figure 2D) increase in MAP pre-surgery and six days post-AVF surgery. The exact systolic and diastolic blood pressure measurements in $Pkd1^{t/t}$ mice are shown in supplemental figure 1.

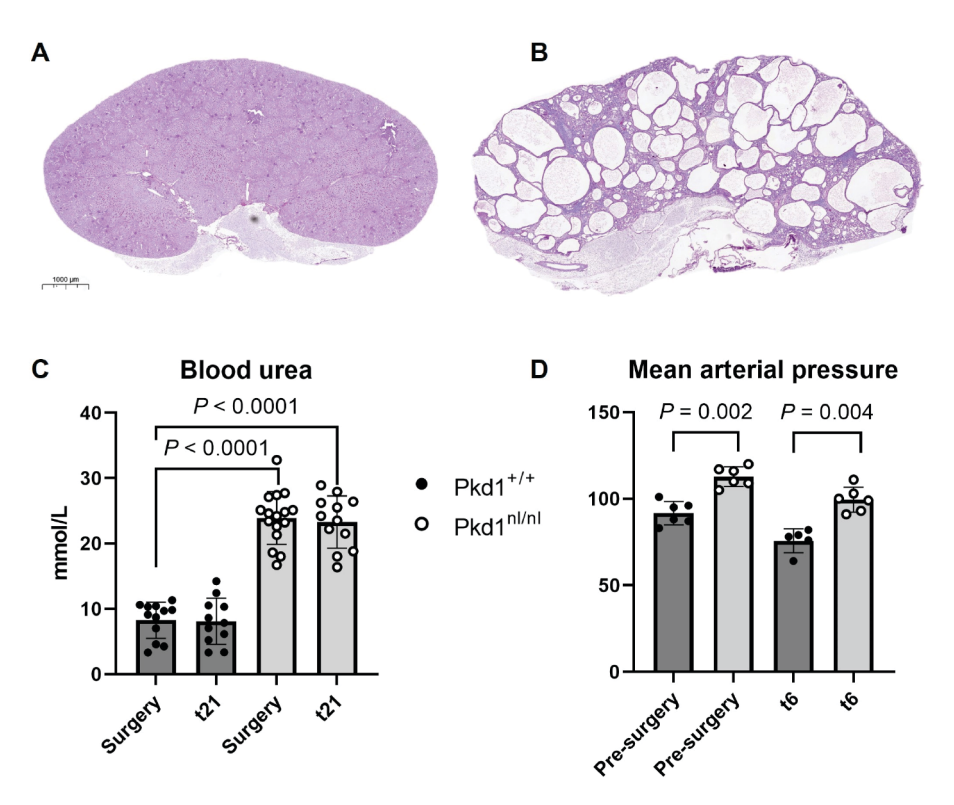


Figure 2: Kidney function and blood pressure in the mouse model. Periodic acid-Schiff (PAS) staining of a healthy Pkd1*/* (A) and Pkd1*/* polycystic kidney (B). Pkd1*/* mice have increased blood urea levels throughout the 21-day study period (C), and hypertension pre-surgery and six days post AVF creation (D). Data is expressed as mean ± SD. ADPKD = Autosomal dominant polycystic kidney disease

Disturbed venous ECM remodelling in AVFs of Pkd1^{nl/nl} mice

To determine early vascular response and which pathways cascade the vascular remodelling, bulk poly-A RNA sequencing was performed seven days post-AVF surgery. Differentially expressed (absolute log2 fold change [FC] \geq 1, adjusted p-value \leq 0.05) processes of vascular remodelling of the arterial AVF segment were mostly related to oxygen exchange and vascular muscle contraction (Supplemental Figure 2).

The venous outflow tract of AVFs in *Pkd1^{nl/nl}* mice showed several downregulated genes involved in vascular remodelling (*Flt4, Tbx1, Olfml3*, Figure 3A), and the ECM (extracellular matrix: *Col11A1, Tnc, Tnn* and *Acan*). Genes related to mechanical tension (*Palmd, Ablim1*) were upregulated. Gene set enrichment analyses of DEGs (figure 3B) indeed demonstrated transcriptional activation of muscle contraction (vasoconstriction), whereas transcription of processes involved in ECM regulation was inhibited in *Pkd1^{nl/nl}* mice. IPA pathway analysis (supplemental table 1) revealed upregulation of transcription factors Gata6, Sox2, Smarca2, Npm1 and Esrra and cytokines CSF1 and IL-13. To verify RNA-sequencing findings at 21 days post AVF-surgery, murine AVFs were stained for Tenascin-C and VEGFR3 which is encoded by Flt4 (figure 4). Although not statistically significant, we see a similar trend on both day 7 and 21 post-surgery as observed with RNA sequencing, namely less Tenascin-C and VEGFR3 protein in AVFs of *Pkd1^{nl/nl}* mice compared to *Pkd1^{nl/nl}* mice.

Pkd1^{nl/nl} mice have increased AVF flow

Blood flow in the CCA proximal to the site of anastomosis was assessed weekly via ultrasonography. $Pkd1^{nl/nl}$ and $Pkd1^{nl/nl}$ mice had comparable flow volume presurgery (figure 5A), whereafter AVF flow was increased in both groups over the 21-day study period (time p<0.0001). $Pkd1^{nl/nl}$ mice show increased AVF flow volume compared to $Pkd1^{nl/nl}$ mice (group effect p=0.001), with an increase in both peak and mean blood velocity (figure 5B) but not increased luminal area of the CCA compared to $Pkd1^{nl/nl}$ mice (figure 5C). To verify whether hypertension and increased flow velocity in the ADPKD model was caused by vascular stiffness, the maximum acceleration (ACCmax) in the CCA was determined. However, no increase in systolic ACCmax over time nor a group difference between $Pkd1^{nl/nl}$ and $Pkd1^{nl/nl}$ and $Pkd1^{nl/nl}$ mice (figure 5D) was observed. Male and female mice were also analysed separately and showed similar differences between $Pkd1^{nl/nl}$ and $Pkd1^{nl/nl}$ mice (supplemental figure 3).

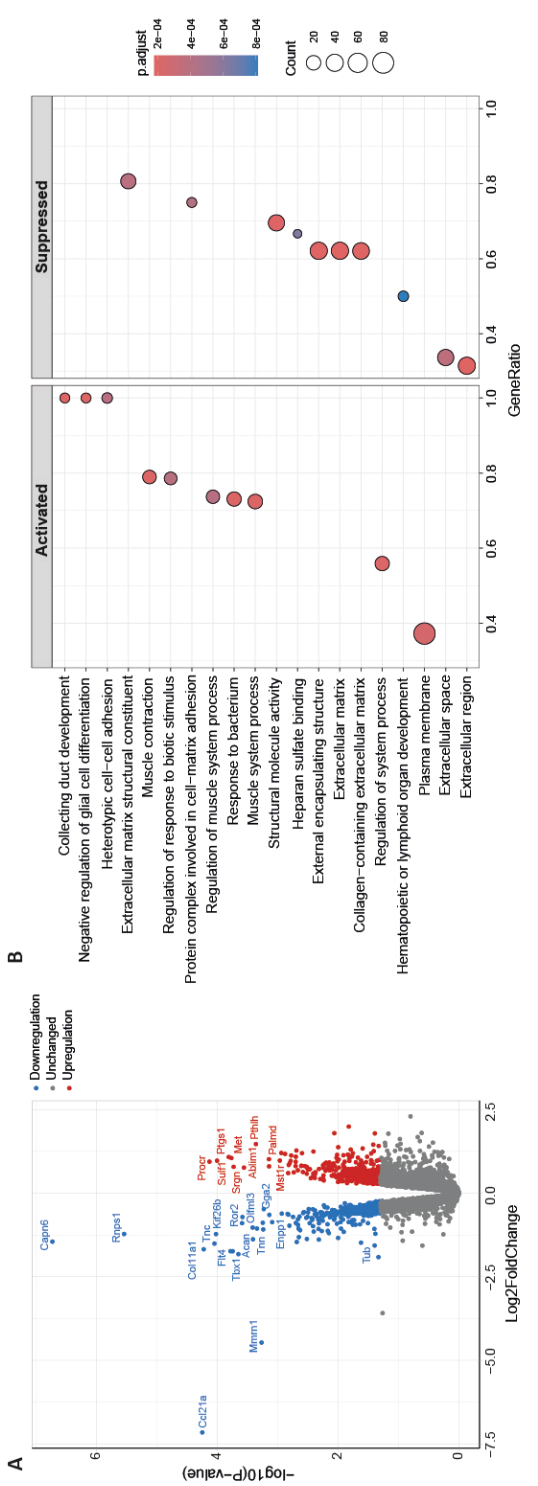


Figure 3: DEGs and functional pathways in the venous AVF segment. (A) Volcano plot representation of DEGs in the venous AVF outflow tract of PKd1^{n/n/n} mice in pairwise comparisons with Pkd1**mice. Changes in gene expression are presented as log10 fold change, red dots indicate upregulated genes in AVFs (B) Pathway enrichment analyses of DEGs using Gene Ontology, showing activated and suppressed biological processes of AVF induced venous remodelling with Pkd1" mice as a reference control for gene expression in Pkd1" mice. Gene ratio indicates the ratio of DEGs in an annotated term over all genes in (log2 fold change \geq 1, adjusted p-value < 0.05), and blue dots are genes downregulated in Pkd1^{n(M)} fistulas (log2 fold change \leq -1, adjusted p-value < 0.05). this term. DEG = Differentially expressed gene.

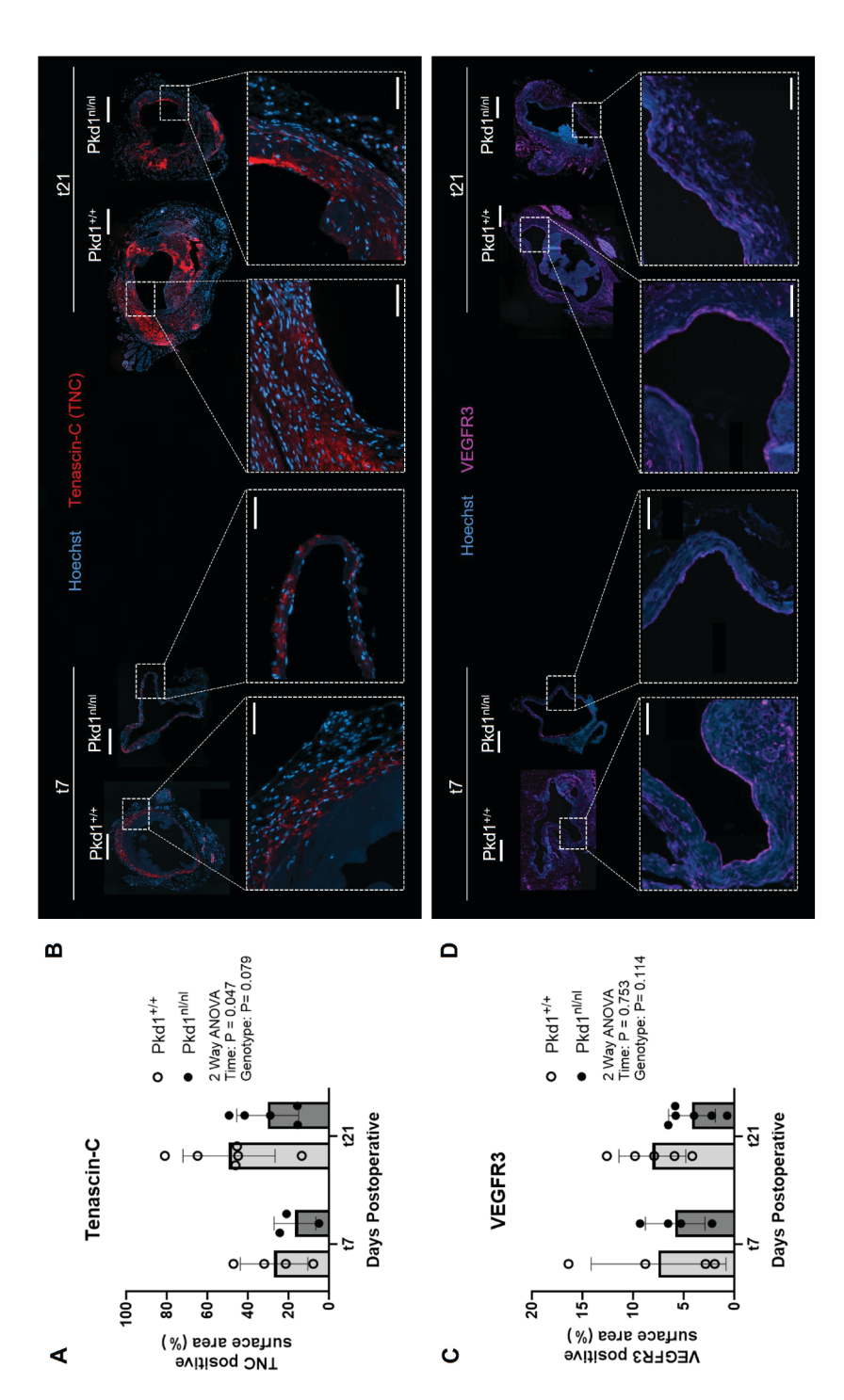


Figure 4: Quantitative analysis of Tenascin-C and VEGFR3. (A) Quantification of Tenascin-C (TNC) in Pkd1** and Pkd1*** and 2 and 21 days postoperatively. (B) Representative images of Tenascin-C quantification. (C) Quantification of VEGFR3 in Pkd1** and Pkd1*** (D) Representative images of VEGFR3 quantification. Scale bars represent 200 µm in the full vein images and 50 µm in the magnified insets.

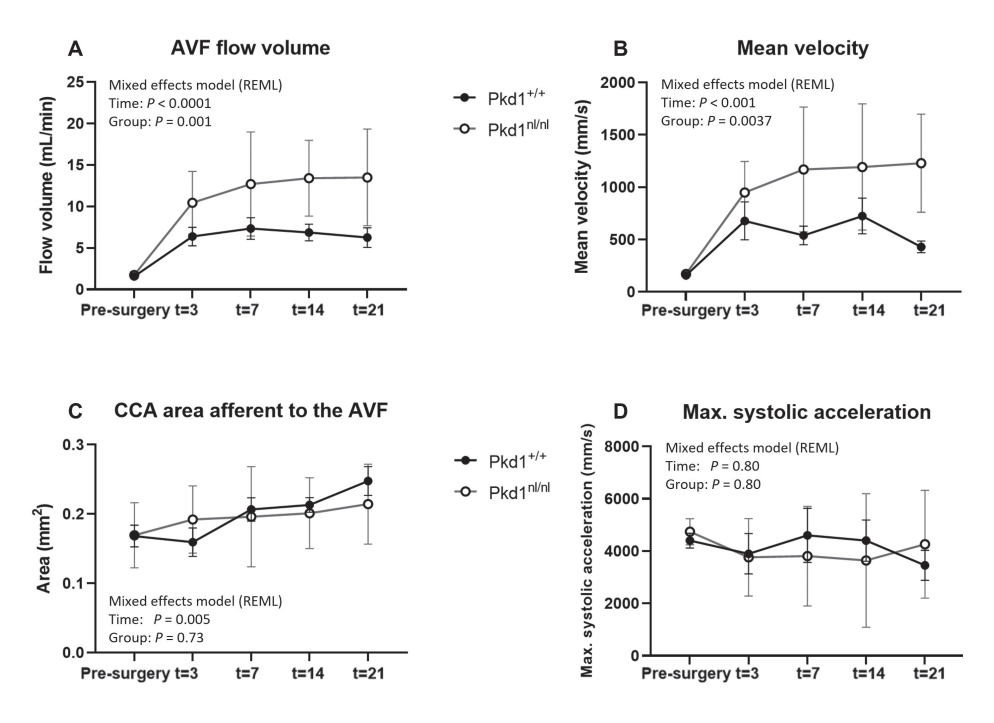


Figure 5: Flow dynamics of the AVF through ultrasound analysis. Blood flow though the AVF increased over time in both groups (A), with significantly higher flow in the $Pkd1^{nl/nl}$ mice due to increased velocity (B). There was no difference in the luminal area of the common carotid artery (CCA) afferent to the AVF anastomosis (C) or maximum systolic acceleration (D) between the two groups. T represents the number of days post-AVF surgery, data is expressed as mean \pm SD, n=12 Pkd1^{nl/nl} mice and n=10 Pkd1^{+/+} mice. AVF = arteriovenous fistula

Pkd1^{nl/nl} mice have reduced IH and increased luminal AVF volume

To assess the result of the vascular remodelling process at a stable phase, histological and morphological analysis (figure 6A) of the AVF were performed on samples obtained twenty-one days post-AVF surgery. The venous outflow tract of the AVF of $Pkd1^{nl/nl}$ mice showed a 50% reduction in IH (figure 6B, p = 0.03) and 40% reduction of total vessel wall area (figure 6C, p = 0.02). Ultrasound analysis showed a 28% increase in luminal volume of the venous outflow tract of $Pkd1^{nl/nl}$ mice compared to $Pkd1^{nl/nl}$ mice (figure 6D & E, p = 0.04). Sex-specific analyses showed similar trends between $Pkd1^{nl/nl}$ and $Pkd1^{nl/nl}$ mice (supplemental figure 4).

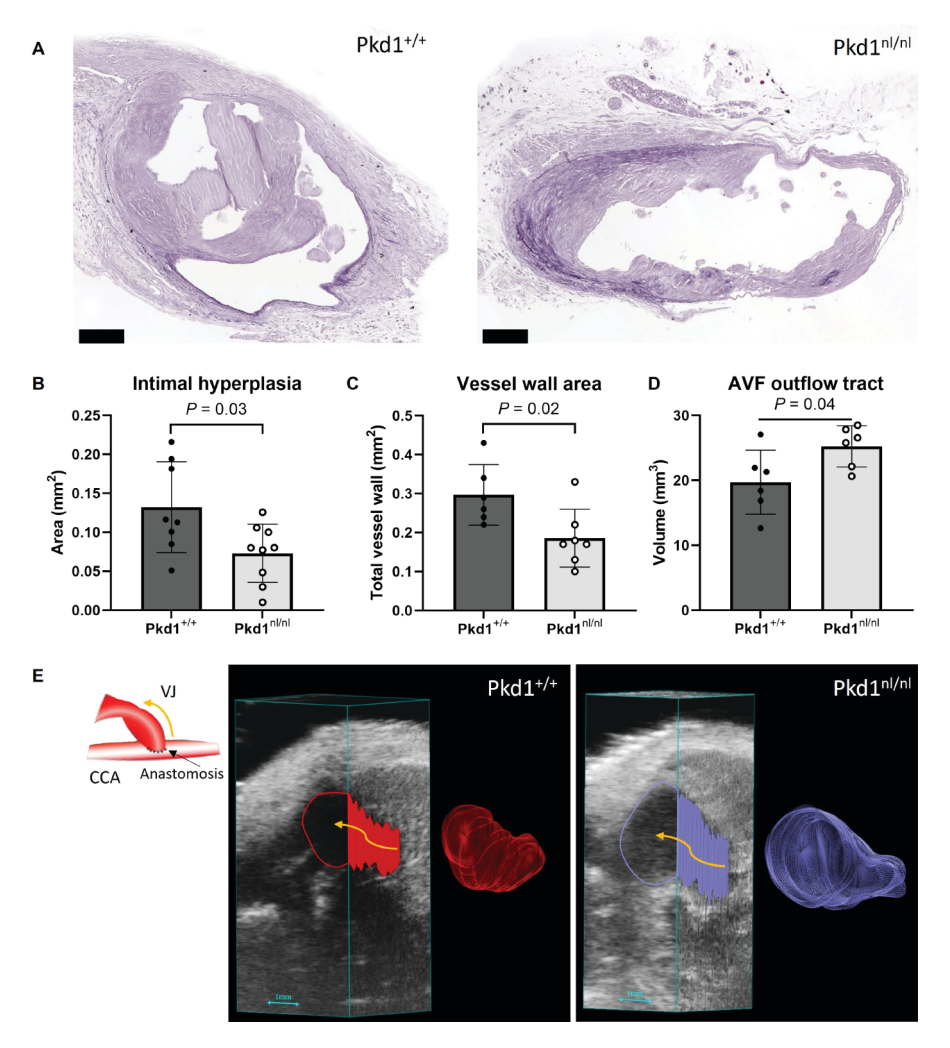


Figure 6: Morphometric analysis of the AVF 21 days post-surgery. (A) Weigert's Elastin staining of the venous outflow tract representative of Pkd1 $^{+/+}$ (left panel) and Pkd1 $^{nl/nl}$ (right panel) mice. The black scale bar indicates 100 µm. Pkd1 $^{nl/nl}$ mice have decreased intimal hyperplasia formation (B), and a smaller vessel wall area (C). Analysis of the luminal volume of the AVF outflow tract from ultrasound analysis showed an increased venous luminal volume in Pkd1 $^{nl/nl}$ AVFs at 21 days post AVF surgery (D). Data is expressed as mean \pm SD. (E) Visual of the AVF anatomy (left panel) and representative images of volumetric measurements and corresponding 3D renders of the venous limb of the AVF in Pkd1 $^{+/+}$ and Pkd1 $^{nl/nl}$ mice. Volume is standardised over the first 2.5 mm from the anastomosis, represented by the yellow arrow. CCA = common carotid artery, VJ = yena jugularis

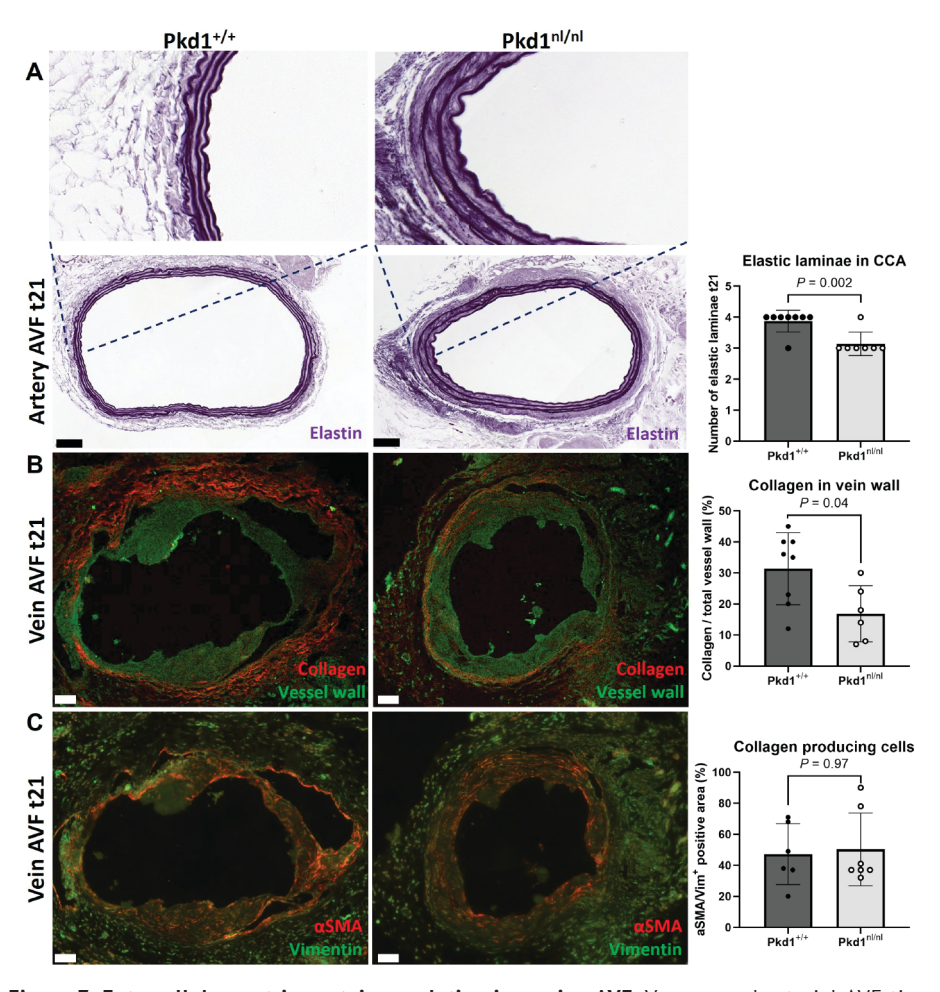


Figure 7: Extracellular matrix protein regulation in murine AVF. Venous and arterial AVF tissue harvested 21 days post-AVF creation. Weigert's elastin stain of the afferent AVF artery (A) shows a loss of elastic laminae in the Pkd1^nl/nl vessel with deposition in between the laminae, top figures are higher magnifications. Second harmonic generation on the venous outflow tract (B) showing diminished collagen deposition (band-pass emission filter at 380-430 nm for collagen in red) in the Pkd1^nl/nl venous outflow tract. The presence of α SMA or Vimentin positive collagen producing cells was comparable in the venous outflow tract of both groups (C). Data is expressed as mean \pm SD. Scale bar indicates 50 μ m.

Pkd1^{nl/nl} mice show reduced extracellular matrix deposition in the AVF

We evaluated the afferent artery for aberrant morphology of the elastic lamina to monitor for potential dilatory effects and the venous outflow tract for collagen deposition . The CCA in $Pkd1^{nl/nl}$ mice displayed a reduction in the number of elastic lamina (figure 7A, p = 0.002), despite having similar elastic laminae pre-surgery. Moreover, the venous AVF outflow tract of $Pkd1^{nl/nl}$ mice showed a 2.2 fold decrease in collagen deposition comparatively to the vessel wall area (figure 7B, p = 0.04), which could not be explained by a reduction of collagen producing vascular cells (α SMA or Vimentin positive cells, figure 7C, p = 0.97) since comparable values between $Pkd1^{nl/nl}$ and controls (median 45% versus 37%, p = 0.97) were observed. Sex-specific analyses showed similar differences in the number of elastic laminae in the CCA and collagen in the vein wall (supplemental figure 5).

Renal arteries of ADPKD patients show ECM dysregulation

We obtained renal arteries of patients undergoing a nephrectomy to investigate ECM deposition in the vasculature of ADPKD patients. Masson trichrome and Weigert's elastin staining (Figure 8) of the renal arteries of controls with a normal kidney function and patients with ADPKD showed dysregulation of ECM deposition and loss of elastic lamina integrity of the renal artery of patients with chronic kidney failure.

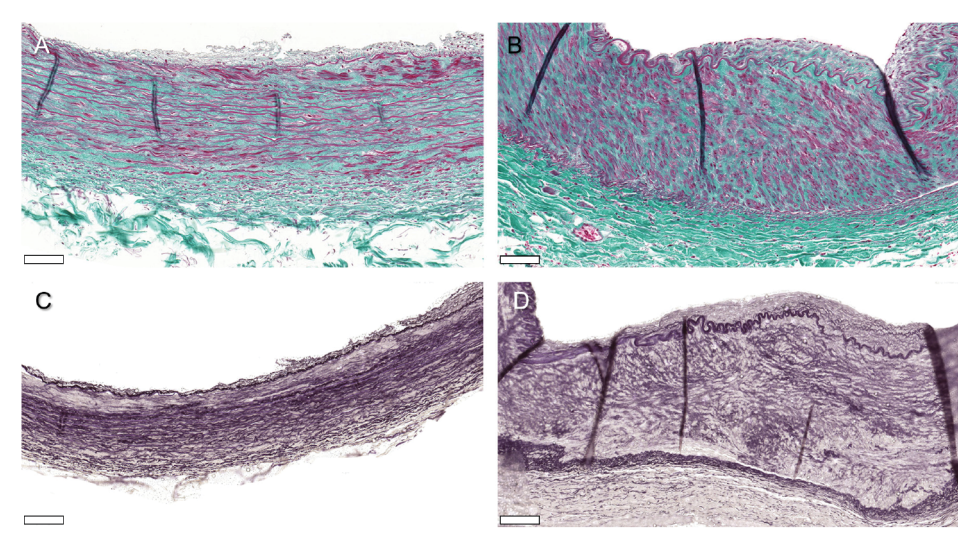


Figure 8: Extracellular matrix in the human renal artery. Masson Trichrome staining of a renal artery from a patient with normal kidney function (A) and ADPKD patient (B) indicates dysregulated extracellular matrix deposition in human ADPKD vessels. This is also shown by samples stained with Weigert's elastin, where compared to the healthy control (C), ADPKD vessels show loss of integrity of the elastin fibres (D). Scale bar indicates 100 μm ADPKD = Autosomal dominant polycystic kidney disease.

Discussion

In addressing the need for a chronic preclinical model reflective of ESKD patients undergoing AVF surgery, we utilised an Autosomal Dominant Polycystic Kidney Disease (ADPKD) model to study AVF maturation in a murine CKD setting.

Pkd1^{nl/nl} mice had increased AVF blood flow, with larger venous outflow tracts. We demonstrated that the increase in luminal AVF volume is due to a combination of increased blood pressure, diminished IH and dysregulated extracellular matrix deposition. IPA pathway analysis revealed upregulation of transcription factors Gata6, Sox2, Smarca2, Npm1 and Esrra and cytokines CSF1 and IL-13, suggesting enhanced vascular remodeling, increased (smooth muscle) cellular proliferation, an altered immune response, and metabolic activation in the ADPKD model [16-22]. Altered ECM remodelling in mice with ADPKD was observed, both during early remodelling using RNA sequencing, and at the endpoint of our study on a histological level. Pkd1^{nl/nl} AVFs showed downregulation of Col11A1, Tnc, Tnn and Acan in the first week post-AVF surgery, which are related to ECM interaction and organisation [23-26]. This was followed at the later time point by disruption of arterial elastin and decreased venous collagen deposition. The ECM is also proven essential in clinical AVF remodelling: Martinez et al.[27] demonstrated that failed and matured AVFs can be categorised by distinct clusters of differentially expressed ECM components. Pathway enrichment analysis revealed a significant increase in collagen remodelling, both degradation and production, from preaccess veins to pair-matched brachiobasilic AVFs of ESKD patients. AVF maturation is characterised by phases of ECM degradation, reorganisation of the collagen and elastin scaffold, and deposition of ECM proteins [28, 29].

Although murine studies show the importance of hindering elastin deposition [30, 31], direct elastin inhibition in randomized double-blind placebo-controlled trials did not have an effect on AVF venous diameter, stenosis, blood flow or maturation rates [32, 33]. This indicates that solely increasing elastin degradation might not be of therapeutic value to improve maturation and AVF patency. In contrast, inhibiting lysyl oxidase (LOX), which aids crosslinking of collagen and elastin fibres, had beneficial effects on fibrosis, vessel distensibility and OR of AVFs in rats [34, 35]. Concurrently, pre-access veins of ESKD patients that had higher LOX expression were associated with AVF failure [34]. During early AVF remodelling, RNA sequencing analysis showed disturbed venous ECM remodelling, later on followed by decreased collagen expression in the venous outflow tract and disrupted elastin matrix in the afferent artery in *Pkd1*^{nl/nl} mice. This altered vascular remodelling might be essential for the increase in luminal AVF volume,

vessel distensibility and increase in flow. Excessive ECM degradation or inadequate repair however can lead to a weakened or even aneurysmal AVF [29], stressing the importance of balanced ECM degradation followed by deposition.

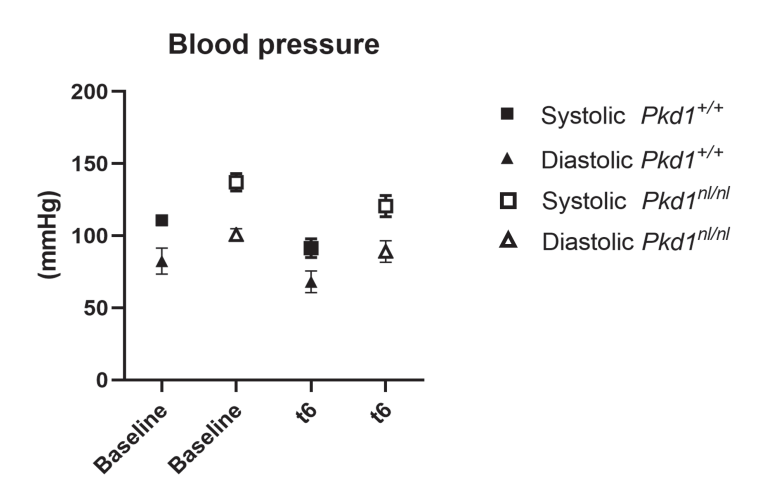
Studying AVF outcomes in other, although more acute, kidney-failure models, Song et al. [36] observed that 5/6th nephrectomy caused vascular fibrosis due to increased myofibroblast differentiation and intimal-ECM. Secondly, Kang et al. [3] detected increased MMP-9 and TGF-B1 expression in the AVFs in a similar model. Overall, compared to acute renal failure model studies, chronic kidney failure in the form of ADPKD had a differential effect on AVF outcome in general. Surgically or diet-induced loss of kidney function mainly resulted in hindered AVF flow and enhanced formation of IH in rats and mice [2-7, 11, 37]. Some attributed AVF failure in their models on EC related processes such as loss of vascular endothelial-cadherin expression and delayed regeneration of the endothelium [37], oxidative stress [2] and impaired dilatation of both the afferent artery and downstream venous outflow tract [7]. Others observed excessive IH formation due to increased VSMC migration and downregulation of contractile VSMC markers α -actin and calponin [5, 11]. In our CKD model however, there was no effect on collagen producing cells such as VSMCs and fibroblast. Instead, combined hypertension and uraemia resulted in decreased IH formation and ECM deposition, leading to increased AVF venous outflow tract volume and AVF flow.

ADPKD is associated with a higher incidence of aneurysm incidences, mainly intracranial and abdominal [38-41], but also a higher frequency of AVF aneurysms compared to other patients with ESKD has been reported [42]. This could be due to altered vasculopathy. 93% of patients with polycystic kidney disease have a mutation in the PKD1 or PKD2 gene, encoding Polycystin-1 and -2, and the remaining 7% has an undiagnosed mutation or one in a gene involved in polycystin protein regulation.[43-48] Polycystin-1 and -2 interact to form an ion channel complex regulating calcium influx, involved in sensing mechanotransduction and fluid flow [49, 50]. PKD1, which is affected in our mouse model [12], is expressed in both endothelial cells (ECs) and vascular smooth muscle cells (VSMCs) and is essential to maintain vessel wall integrity [51, 52]. Reduced Pkd1 expression in VSMCs causes the threshold pressure for myogenic contraction to go up [53] and induces phenotypic switching and affects the extracellular matrix [54-56]. This can explain the decreased ECM organisation in the AVF of $Pkd1^{nl/nl}$ mice. It is important to note that we did not observe either venous or arterial AVF aneurysm formation, as there was no significant increase in the diameter of the CCA afferent to the AVF and we observed a thicker venous wall, strengthened by increased collagen deposition. However, we cannot rule out the possibility of aneurysm formation over a longer time frame. Additionally, our model may be influenced by general CKD as well as ADPKD-specific effects, which poses an interesting research question for further studies. Nonetheless, our model is a clinical representative model for a substantial portion of patients with an AVF, as patients with ADPKD comprise approximately 9% of patients requiring kidney replacement therapy, and 69% of this patient group undergoes HD [57]. The majority of patients with ADPKD on HD utilize an AVF as vascular access [58]. The question arises if the observed differences in AVF remodelling primarily relate to the impaired kidney function or if they are specific for ADPKD. In this respect, it is important to notice that in our recent clinical study, patency rates of AVF/AVG in ADPKD patients were similar to those of ESKD patients with other primary kidney disease [59]. This suggests that ADPKD does not affect AVF outcomes differently than other causes of ESKD, reinforcing the representativeness of our ADPKD model for ESKD patients receiving AVFs.

In conclusion, our study introduced a novel *in vivo* model suitable to study AVF remodeling in the setting of chronic kidney disease, resulting in improved AVF maturation in mice with ADPKD, as illustrated by enhanced luminal volume and higher AVF flow. Moreover, this ADPKD model holds promise for investigating the effects of hypertension, uraemia, and interventions targeting the ECM in AVF remodelling.

Supplemental material

Supplemental Figs. S1–S5 and Table S1 can be found at: https://doi.org/10.6084/m9.figshare.29433362



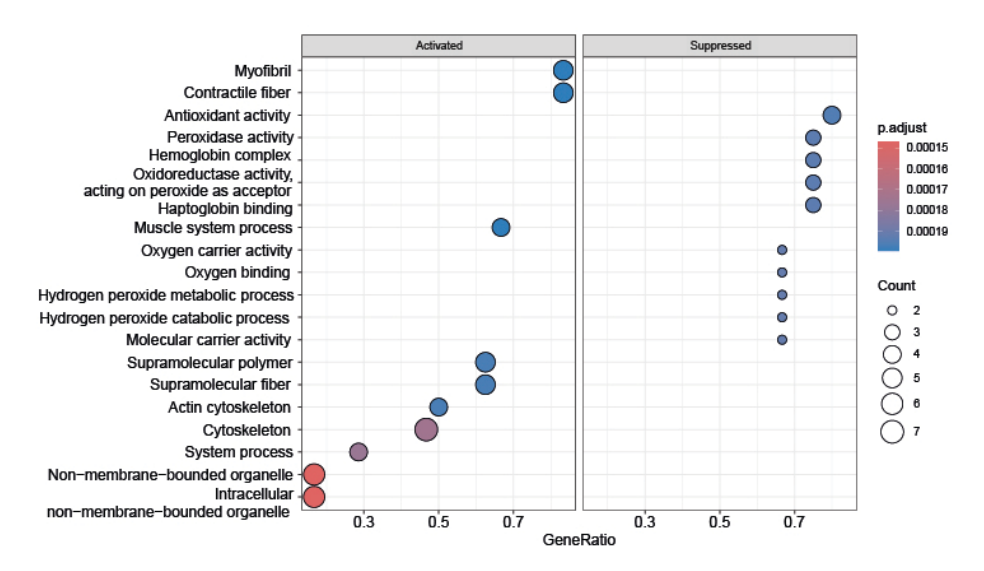
Supplemental figure 1: Systolic and diastolic blood pressure

Systolic (box) and diastolic (triangle) blood pressure measured before AVF creation (baseline) and six days post-surgery (t6). N=6 mice per group.

Supplemental table 1: IPA analysis of upstream factors involved in the DEGs and functional pathways

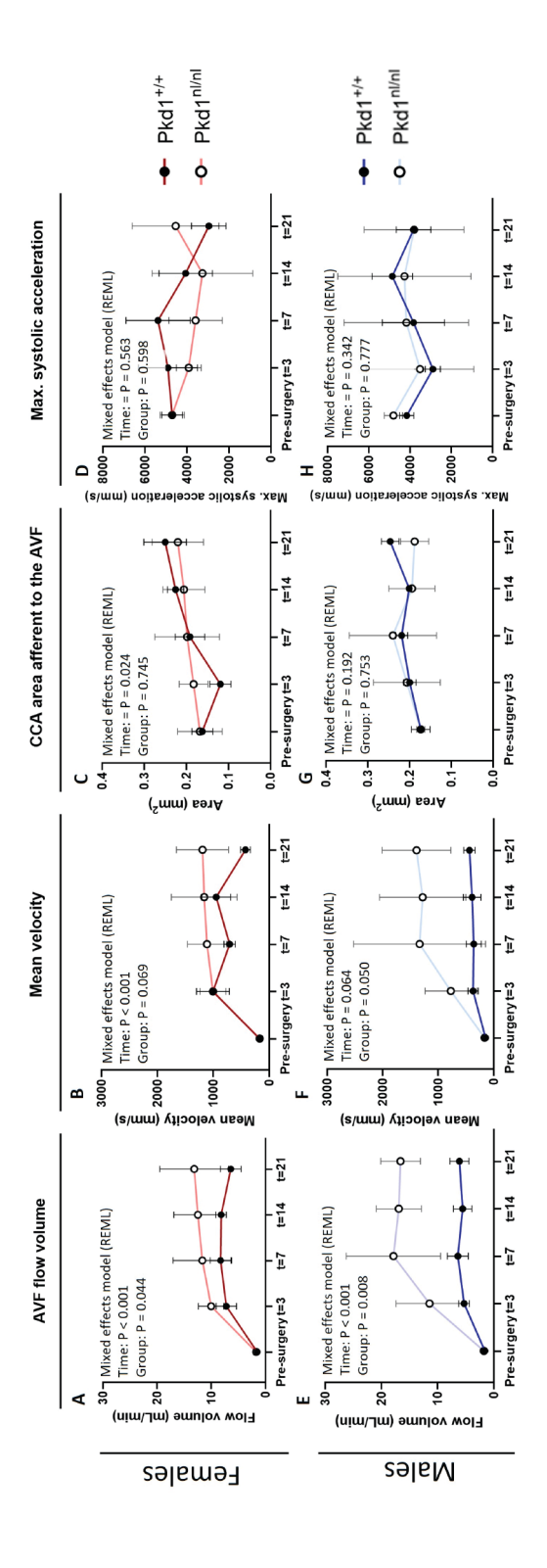
Upstream Regulator	Activation z-score	p-value	Target molecules in dataset	Category
GATA6	2,4	0,0000174	BMP4, DLK1, DPP4, LYVE1, PTGS1, SEMA3C	Transcription Factor
SOX2	2,4	0,000276	ACKR3, BMP4, H19, MBP, PARD6G, SPP1, TMEM100	Transcription Factor
SMARCA2	2,0	0,000027	BMPR1B, COL11A1, IGFBP5, MBP	Transcription Factor
NPM1	2,0	0,00085	IGFBP5, NR1D1, PCOLCE2, PTHLH	Transcription Factor
CSF1	2,0	0,00187	GPNMB, ITGAX, LYVE1, Retnla, SPP1	Cytokine
IL13	2,0	0,0000333	ACKR3, FGFR3, FLT4, GPNMB, ITGAX, NTN1, Retnla, SPP1	Cytokine
ESRRA	2,0	0,0171	ACKR3, ATP1A3, NR1D1, SPP1	Transcription Factor
MYC	-2,2	0,0248	ACAN, H19, ITGAX, MBP, PTHLH, PTN, SPP1, TNC	Transcription Factor

An overview of transcription factors and cytokines that are significantly altered ($-2 \le z$ -score ≥ 2), and the accompanying target molecules, with Pkd1^{+/+} mice as a reference control for gene expression in Pkd1^{nl/nl} mice. DEG = differentially expressed gene, IPA = ingenuity pathway analysis.

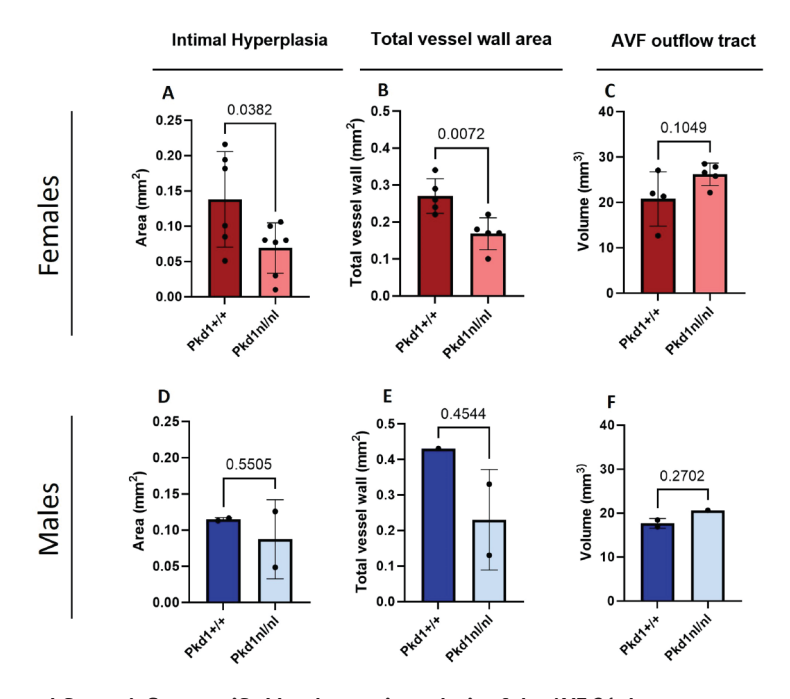


Supplemental figure 2: Functional pathways in the arterial AVF segment

Pathway enrichment analyses of DEGs using Gene Ontology, showing activated and suppressed biological processes of AVF induced arterial remodelling with Pkd1**/* mice as a reference control for gene expression in Pkd1**/*Imice. Gene ratio indicates the ratio of DEGs in an annotated term over all genes in this term. DEG = Differentially expressed gene.

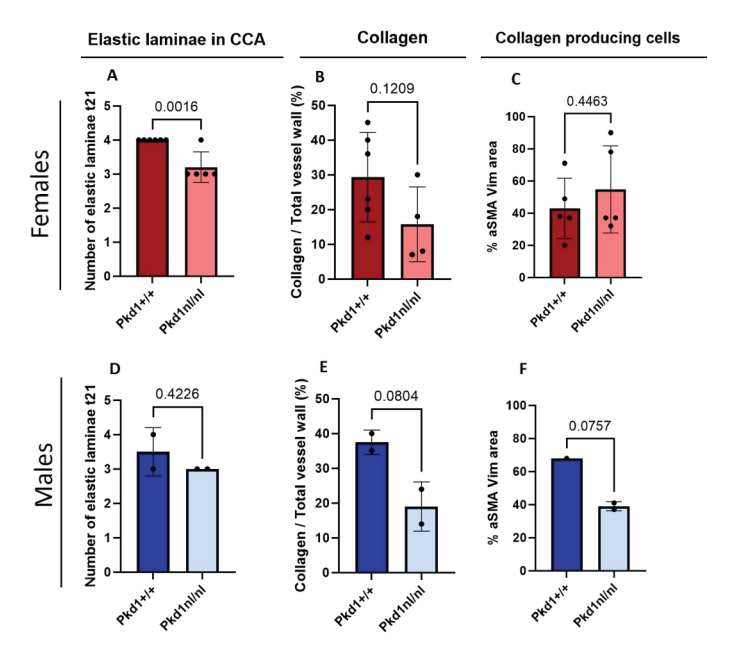


Blood flow and blood flow velocity over the AVF increased over time and was consistently higher postoperatively in the in the Pkd1" mice in both males not differ between groups (D, G). There was no difference in maximum systolic acceleration over time or between groups. T represents the number of days and females (A, B, E, F). The increase in luminal area of the common carotid artery (CCA) over time was only statistically significant in female mice and did Supplemental figure 3: Sex-specific flow dynamics of the AVF through ultrasounds analysis post-AVF surgery, data is expressed as mean ± SD. AVF = arteriovenous fistula.



Supplemental figure 4: Sex-specific Morphometric analysis of the AVF 21 days post-surgery Female Pkd1^{nl/nl} mice have decreased intimal hyperplasia formation (A), and a smaller vessel wall

Female Pkd1^{nl/nl} mice have decreased intimal hyperplasia formation (A), and a smaller vessel wall area (B). Analysis of the luminal volume of the AVF outflow tract showed an increased venous luminal volume in Pkd1^{nl/nl} AVFs at 21 days post AVF surgery but lacked statistical significance when performing separate analyses for each sex (D). Morphometric differences between groups were similar in male mice, however there was insufficient power to assess statistical significance in male mice, p value is included for reference (D-F). Data is expressed as mean ± SD.



Supplemental figure 5: Sex-specific analyses of extracellular matrix protein regulation

Male and female Pkd1^{nl/nl} mice show decreased number of elastic laminae but only females had sufficient numbers to determine statistical significance, p value for the male groups is included for reference. Second harmonic generation on the venous outflow tract shows diminished collagen deposition in the Pkd1^{nl/nl} venous outflow tract in both female and male mice (B, E) but lacked statistical significance when analysed separated by sex. α SMA or Vimentin positive collagen producing cells did not differ between groups (C, F). Data is expressed as mean \pm SD.

Disclosures

All authors declared no competing interests.

References

- Shiu, Y.T., et al., Arteriovenous conduits for hemodialysis: how to better modulate the pathophysiological vascular response to optimize vascular access durability. Am J Physiol Renal Physiol, 2019. 316(5): p. 13. F794-f806.
- Geenen, I.L., et al., Nitric Oxide Resistance Reduces Arteriovenous Fistula Maturation in Chronic Kidney Disease in Rats. PLoS One, 2016. 11(1): p. e0146212.
- Kang, L., et al., A new model of an arteriovenous fistula in chronic kidney disease in the mouse: beneficial effects of upregulated heme oxygenase-1. American Journal of Physiology-Renal Physiology, 2016. 310(6): p. F466-F476.
- 4. Zheng, C., et al., Establishment of a rat autogenous arteriovenous fistula model following 5/6 nephrectomy. Exp Ther Med, 2015. 10(1): p. 219-224.
- Ferrer, L.M., et al., Caspase-1 Plays a Critical Role in Accelerating Chronic Kidney Disease-Promoted Neointimal Hyperplasia in the Carotid Artery. J Cardiovasc Transl Res, 2016. 9(2): p. 135-44.
- Croatt, A.J., et al., Characterization of a Model of an Arteriovenous Fistula in the Rat: The Effect of L-NAME. The American Journal of Pathology, 2010. 176(5): p. 2530-2541.
- Langer, S., et al., Chronic kidney disease aggravates arteriovenous fistula damage in rats. Kidney International, 2010. 78(12): p. 1312-1321.
- Khattri, R.B., et al., Metabolomic profiling reveals muscle metabolic changes following iliac arteriovenous fistula creation in mice. Am J Physiol Renal Physiol, 2022. 323(5): p. F577-f589.
- Rezapour, M., et al., Less primary fistula failure in hypertensive patients. Journal of Human Hypertension, 2018. 32(4): p. 311-318.
- Wang, K., et al., Effect of Anti-Hypertensive Medication History on Arteriovenous Fistula Maturation Outcomes. American Journal of Nephrology, 2018. 48(1): p. 56-64.
- **11.** Kokubo, T., et al., CKD accelerates **22.** development of neointimal hyperplasia in arteriovenous fistulas. J Am Soc Nephrol, 2009. **20**(6): p. 1236-45.

- Happé, H., et al., Cyst expansion and regression in a mouse model of polycystic kidney disease. Kidney International, 2013. 83(6): p. 1099-1108.
- Lantinga-van Leeuwen, I.S., et al., Lowering of Pkd1 expression is sufficient to cause polycystic kidney disease. Hum Mol Genet, 2004. 13(24): p. 3069-77.
- Wong, C.Y., et al., A Novel Murine Model of Arteriovenous Fistula Failure: The Surgical Procedure in Detail. J Vis Exp, 2016(108): p. e53294.
- 15. Laboyrie, S.L., et al., von Willebrand Factor: A Central Regulator of Arteriovenous Fistula Maturation Through Smooth Muscle Cell Proliferation and Outward Remodeling. Journal of the American Heart Association, 2022. 11(16): p. e024581.
- 16. Kopp, J.L., et al., Small increases in the level of Sox2 trigger the differentiation of mouse embryonic stem cells. Stem Cells, 2008. 26(4): p. 903-11.
- Yin, F. and B.P. Herring, GATA-6 can act as a positive or negative regulator of smooth muscle-specific gene expression. J Biol Chem, 2005. 280(6): p. 4745-52.
- 18. Wu, W., et al., Endothelial Gata6 deletion reduces monocyte recruitment and proinflammatory macrophage formation and attenuates atherosclerosis through Cmpk2-Nlrp3 pathways. Redox Biol, 2023. 64: p. 102775.
- Liu, H., et al., SWI/SNF Complex in Vascular Smooth Muscle Cells and Its Implications in Cardiovascular Pathologies. Cells, 2024. 13(2): p. 168.
- Rao, C., et al., Nucleophosmin contributes to vascular inflammation and endothelial dysfunction in atherosclerosis progression. J Thorac Cardiovasc Surg, 2021. 161(5): p. e377-e393.
- Sopariwala, D.H., et al., Estrogen-related receptor α is involved in angiogenesis and skeletal muscle revascularization in hindlimb ischemia. Faseb j, 2021. 35(5): p. e21480.
- Sumi, D. and L.J. Ignarro, Estrogen-related receptor alpha 1 up-regulates endothelial nitric oxide synthase expression. Proc Natl Acad Sci U S A, 2003. 100(24): p. 14451-6.

- 23. Sun, M., et al., Collagen XI regulates the 33. acquisition of collagen fibril structure, organization and functional properties in tendon. Matrix Biology, 2020. 94: p. 77-94.
- 24. Giuffrida, A., et al., The interaction of tenascin-C with fibronectin modulates the 34. migration and specific metalloprotease activity in human mesothelioma cell lines of different histotype. Int J Oncol, 2004. 25(3): p. 745-50.
- Jones, P.L., et al., Induction of vascular smooth muscle cell tenascin-C gene expression by denatured type I collagen is dependent upon a β3 integrin-mediated mitogen-activated protein kinase pathway and a 122-base pair promoter element. Journal of Cell Science, 1999. 112(4): p. 435-445.
- Suna, G., et al., Extracellular Matrix Proteomics Reveals Interplay of Aggrecan and Aggrecanases in Vascular Remodeling of Stented Coronary Arteries. Circulation, 2018. 137(2): p. 166-183.
- Martinez, L., et al., The Transcriptomics of the Human Vein Transformation After Arteriovenous Fistula Anastomosis Uncovers Layer-Specific Remodeling and Hallmarks of Maturation Failure. Kidney International Reports, 2023.
- Hall, M.R., et al., Temporal regulation of venous extracellular matrix components during arteriovenous fistula maturation. J Vasc Access, 2015. 16(2): p. 93-106.
- Laboyrie, S.L., et al., Building a Scaffold for Arteriovenous Fistula Maturation: Unravelling the Role of the Extracellular Matrix. International Journal of Molecular 40. Sciences, 2023. 24(13): p. 10825.
- Wong, C.Y., et al., Elastin is a key regulator of outward remodeling in arteriovenous fistulas. Eur J Vasc Endovasc Surg, 2015. 41.
 49(4): p. 480-6.
- **31.** Bezhaeva, T., et al., Relaxin receptor deficiency promotes vascular inflammation and impairs outward remodeling in arteriovenous fistulas. Faseb j, 2018: p. fj201800437R.
- **32.** Peden, E.K., et al., PATENCY-2 trial of vonapanitase to promote radiocephalic fistula use for hemodialysis and secondary patency. The Journal of Vascular Access, 2022. **23**(2): p. 265-274.

- **33.** Bleyer, A.J., et al., A randomized trial of vonapanitase (PATENCY-1) to promote radiocephalic fistula patency and use for hemodialysis. Journal of Vascular Surgery, 2019. **69**(2): p. 507-515.
- 34. Hernandez, D.R., et al., Inhibition of Lysyl Oxidase with β-aminopropionitrile Improves Venous Adaptation after Arteriovenous Fistula Creation. Kidney360, 2021. 2(2): p. 270-278.
- 35. Applewhite, B., et al., Periadventitial β-aminopropionitrile-loaded nanofibers reduce fibrosis and improve arteriovenous fistula remodeling in rats. Frontiers in Cardiovascular Medicine, 2023. 10.
- Song, K., et al., PDGFRA in vascular adventitial MSCs promotes neointima formation in arteriovenous fistula in chronic kidney disease. JCI Insight, 2020. 5(21).
- 37. Liang, A., et al., Chronic kidney disease accelerates endothelial barrier dysfunction in a mouse model of an arteriovenous fistula. American Journal of Physiology-Renal Physiology, 2013. 304(12): p. F1413-F1420.
- 38. Cagnazzo, F., et al., Intracranial aneurysms in patients with autosomal dominant polycystic kidney disease: prevalence, risk of rupture, and management. A systematic review. Acta Neurochirurgica, 2017. 159(5): p. 811-821.
- Sung, P.H., et al., Risk of aortic aneurysm and dissection in patients with autosomaldominant polycystic kidney disease: a nationwide population-based cohort study. Oncotarget, 2017. 8(34): p. 57594-57604.
- 40. Kato, A., et al., Abdominal aortic aneurysms in hemodialysis patients with autosomal dominant polycystic kidney disease. Nephron, 2001. 88(2): p. 185-6.
- 41. Irazabal, M.V., et al., Extended follow-up of unruptured intracranial aneurysms detected by presymptomatic screening in patients with autosomal dominant polycystic kidney disease. Clin J Am Soc Nephrol, 2011. 6(6): p. 1274-85.
- **42.** Jankovic, A., et al., Arteriovenous Fistula Aneurysm in Patients on Regular Hemodialysis: Prevalence and Risk Factors. Nephron Clinical Practice, 2013. **124**(1-2): p. 94-98.

- disease: the complete structure of the PKD1 gene and its protein. Cell, 1995. 81(2): p. 289-98.
- 44. Mochizuki, T., et al., PKD2, a gene for polycystic kidney disease that encodes an integral membrane protein. Science, 1996. 54 272(5266): p. 1339-42.
- Senum, S.R., et al., Monoallelic IFT140 pathogenic variants are an important cause of the autosomal dominant polycystic kidneyspectrum phenotype. The American Journal of Human Genetics, 2022. **109**(1): p. 136-156. **55**
- 46. Cornec-Le Gall, E., et al., Monoallelic Mutations to DNAJB11 Cause Atypical Autosomal-Dominant Polycystic Kidney Disease. Am J Hum Genet, 2018. **102**(5): p. **56**.
- 47. Porath, B., et al., Mutations in GANAB, Encoding the Glucosidase IIα Subunit. Cause Autosomal-Dominant Polycystic Kidney and Liver Disease. Am J Hum Genet, 2016. **98**(6): **57** p. 1193-1207.
- 48. Besse, W., et al., ALG9 Mutation Carriers Develop Kidney and Liver Cysts. J Am Soc 58. Nephrol, 2019. 30(11): p. 2091-2102.
- 49. Hanaoka, K., et al., Co-assembly of polycystin-1 and -2 produces unique cationpermeable currents. Nature, 2000. 408(6815): p. 990-994.
- 50. Nauli, S.M., et al., Polycystins 1 and 2 mediate 59. mechanosensation in the primary cilium of kidney cells. Nature Genetics, 2003. 33(2): p. 129-137.
- Kim, K., et al., Polycystin 1 is required for the structural integrity of blood vessels. Proc Natl Acad Sci U S A. 2000. 97(4): p. 1731-6.

- 43. Consortium, T.I.P.K.D., Polycystic kidney 52. Griffin, M.D., et al., Vascular expression of polycystin, Journal of the American Society of Nephrology, 1997. 8(4).
 - 53. Sharif-Naeini, R., et al., Polycystin-1 and -2 Dosage Regulates Pressure Sensing, Cell, 2009. **139**(3): p. 587-596.
 - Zhang, J., et al., Polycystin-1 Downregulation Induced Vascular Smooth Muscle Cells Phenotypic Alteration and Extracellular Matrix Remodeling in Thoracic Aortic Dissection. Frontiers in Physiology, 2020. 11.
 - Mangos, S., et al., The ADPKD genes pkd1a/b and pkd2 regulate extracellular matrix formation. Disease Models & Mechanisms, 2010. **3**(5-6): p. 354-365.
 - Drummond, I.A., Polycystins, focal adhesions and extracellular matrix interactions. Biochimica et Biophysica Acta (BBA) - Molecular Basis of Disease, 2011. 1812(10): p. 1322-1326.
 - Astley, M.E., et al., The ERA Registry Annual Report 2020: a summary. Clinical Kidney Journal, 2023: p. sfad087.
 - Budhram, B., et al., End-Stage Kidney Disease in Patients With Autosomal Dominant Polycystic Kidney Disease: A 12-Year Study Based on the Canadian Organ Replacement Registry. Can J Kidney Health Dis, 2018. 5: p. 2054358118778568.
 - Laboyrie, S.L., et al., Vascular Access Outcomes in Patients with Autosomal Dominant Polycystic Kidney Disease. Kidney360, 2024. 5(6).